NMR Spectroscopy

International Edition: DOI: 10.1002/anie.201707114
German Edition: DOI: 10.1002/ange.201707114

Fluorine Pseudocontact Shifts Used for Characterizing the Protein–Ligand Interaction Mode in the Limit of NMR Intermediate Exchange

*Jia Gao[+], E Liang[+], Rongsheng Ma, Fudong Li, Yixiang Liu, Jiuyang Liu, Ling Jiang, Conggang Li, Haiming Dai, Jihui Wu, Xuncheng Su, Wei He, and Ke Ruan**

Abstract: *The characterization of protein–ligand interaction modes becomes recalcitrant in the NMR intermediate exchange regime as the interface resonances are broadened beyond detection. Here, we determined the ^{19}F low-populated bound-state pseudocontact shifts (PCSs) of mono- and di-fluorinated inhibitors of the BRM bromodomain using a highly skewed protein/ligand ratio. The bound-state ^{19}F PCSs were retrieved from ^{19}F chemical exchange saturation transfer (CEST) in the presence of the lanthanide-labeled protein, which was termed the ^{19}F PCS-CEST approach. These PCSs enriched in spatial information enabled the identification of best-fitting poses, which agree well with the crystal structure of a more soluble analog in complex with the BRM bromodomain. This approach fills the gap of the NMR structural characterization of lead-like inhibitors with moderate affinities to target proteins, which are essential for structure-guided hit-to-lead evolution.*

Protein–ligand interaction modes are at the heart of the rational drug discovery campaign. High-throughput screening normally identifies initial lead compounds with mircomolar affinities that are also central to fragment-based drug discovery. The structure-guided optimization of lead compounds requires high-resolution complex crystal structures,[1] but their availability is often limited by the dynamic nature of the targets and/or the low aqueous solubility of the lead compounds. NMR spectroscopy is an alternative and fruitful approach to depict the protein–ligand interaction modes. The interactions between proteins and weak binders in the fast-exchange regime are readily interrogated using NMR chemical shift perturbations,[2] the intermolecular nuclear Overhauser effect (NOE),[3] transferred pseudocontact shifts (PCSs),[4] or transferred paramagnetic relaxation enhancement (PRE).[5] For instance, the ^{1}H PCSs were measured on the excess ligand in fast exchange between free and bound states and used as docking restraints.[4] The lead-like compounds with approximately 10 μM to 10 nM affinities often fall into the NMR intermediate exchange scale, which can cause severe line broadening beyond detection of interface resonances. These issues thus pose an unparalleled challenge to the characterization of protein–ligand interaction modes in the NMR limit of intermediate exchange.[6]

A highly skewed protein–ligand ratio can, in principle, alleviate the line broadening effect because the contribution from chemical exchange is proportional to the product of free and bound-state populations.[7] The chemical shifts of a very low-populated excited or bound state can be intuitively measured by using the chemical exchange saturation transfer (CEST) technique.[8] The ligand-observed ^{1}H CEST may suffer from ^{1}H-^{1}H NOE artifacts,[9] whereas the ^{19}F CEST method presents a clean profile that is free of these interferences. However, it is difficult to build atomic models of the bound state using chemical shifts only. PCSs carry valuable angular and distance information, and have gained increasing interest in the elucidation of protein structure and dynamics, mostly through ^{1}H and ^{15}N PCSs.[10] The ^{19}F PCS was identified for the heme iron of cytochrome P-450 and its fluorinated substrate almost three decades ago,[11] after which fluorinated compounds with a chelating lanthanide were used as contrast agents in magnetic resonance imaging.[12] However, the bound-state ^{19}F PCSs for characterizing the protein–ligand interaction modes remain unexploited. We have recently demonstrated that the ^{15}N CEST profiles of lanthanide-labeled proteins allow the determination of PCSs of the low-populated bound states.[13] Here, we used the ligand-observed ^{19}F CEST in the presence of a low-populated lanthanide-labeled protein to determine the bound-state ^{19}F PCSs (we have dubbed this approach ^{19}F PCS-CEST), which provides valuable structural restraints to delineate the

[*] Dr. J. Gao,[+] Dr. R. Ma, Dr. F. Li, J. Liu, Prof. J. Wu, Prof. Dr. K. Ruan
Hefei National Laboratory for Physical Science at the Microscale, School of Life Science
University of Science and Technology of China
Huangshan Road, Hefei, Anhui 230027 (P. R. China)
E-mail: kruan@ustc.edu.cn
Dr. J. Gao,[+] Prof. Dr. H. Dai
Center of Medical Physics and Technology
Hefei Institute of Physical Science, Cancer Hospital
Chinese Academy of Science, Hefei, Anhui 230031 (P. R. China)
E Liang,[+] Prof. Dr. W. He
Department of pharmacology and Pharmaceutical Sciences
School of Medicine, Tsinghua-Peking Joint centers for Lifer Sciences, Tsinghua University
Beijing, 100084 (P. R. China)
Dr. Y. Liu, Prof. Dr. L. Jiang, Prof. Dr. C. Li
Key Laboratory of Magnet Resonance in Biological Systems, State Key Laboratory of Magnet Resonance and Atomic and Molecular Physics
Wuhan Center for Magnet Resonance Department
Wuhan Institute of Physics and Mathematics
Chinese Academy of Science, Wuhan, Hubei 430071 (P. R. China)
Prof. Dr. X. Su
State Key Laboratory of Elemento-Organic Chemistry
Collatorative Innovation Center of Chemical Science and Engineering(Tianjin) Nankai University, Tianjin 300071, (P. R. China)
[+] These authors contributed equally to this work.
Supporting information and the ORCID identification number(s) for the author(s) of this article can be found under: https://doi.org/10.1002/anie.201707114.

 © 2017 Wiley-VCH Verlag GmbH & Co. KGaA, Weinheim

protein–ligand interaction mode, even in the limit of intermediate exchange.

During our fragment-based lead discovery targeting the bromodomain of BRM, which is closely associated with cardiac hypertrophy[14] and cancers,[15] we identified a micromolar affinity fluorinated inhibitor (**1**) (Figure 1 a). We failed to crystallize the BRM bromodomain in complex with **1**, probably due to the limited aqueous solubility of **1**. A characteristic phenomenon of the intermediate exchange was observed for binding-site residues, for example, L43, V39 and F62, which were beyond detection upon titrating **1** to the 0.2 mM ^{15}N-labeled BRM bromodomain (Figure 1 b). Conversely, ^{19}F spectra of compound **1** become undetectable upon the titration of 50 % or 100 % (molar ratio) BRM bromodomain (Figure 1 c), due to the severe line broadening contributed by the intermediate exchange and the large ^{19}F chemical shift anisotropy of the bound-state ligand. The ^{19}F signal intensity was slightly reduced upon the addition of 2.5 % BRM bromodomain, as the aforementioned line broadening effects were remarkably attenuated by the low population of the bound-state ligand (Figure 1 c).

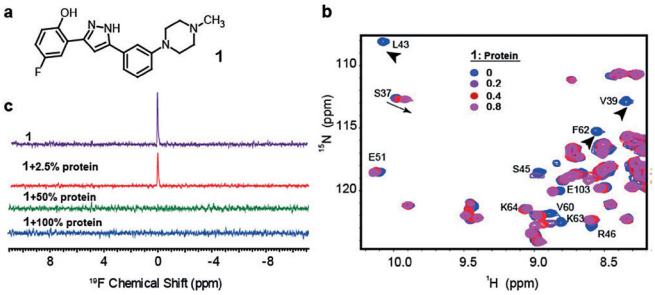

Figure 1. The bound-state signals of interface resonances are beyond detection in the limit of NMR intermediate exchange. a) Chemical structure of the BRM bromodomain inhibitor **1**. b) Residues in the acetyl-lysine recognition pockets of the BRM bromodomain become invisible upon the titration of **1**. c) The ^{19}F signal of **1** retains its sensitivity in the presence of a low-populated BRM bromodomain.

For paramagnetic labeling on the protein, we first introduced a site-specific lanthanide chelator 4MMPyMTA[13] to the BRM bromodomain. The only cysteine residue (C88) of the BRM bromodomain was first mutated to alanine, and this C88A mutant exhibited a heteronuclear single-quantum correlation (HSQC) spectrum similar to that of the wild-type BRM bromodomain (see Figure S1a, S1b in the Supporting Information). Two additional residues (K64 and L86) were then individually mutated to cysteine, as these residues were at least 5 Å away from the binding pocket (Figure S1c); thus, the covalent linking to a lanthanide chelator 4MMPyMTA via a disulfide bond would not perturb the binding site residues. In practice, we prefer to select a lanthanide chelating point approximately 10–20 Å away from the binding pocket (Figure S1c), as it would induce sizeable PCSs of nuclei of interest with moderate paramagnetic relaxation enhancement.[16] The conserved HSQC pattern of these two mutants upon mutagenesis and covalent modification (Figure S1a, S1b) indicate that the global structure of the BRM bromodomain remained untouched.

The ^{15}N PCSs of the BRM bromodomain were measured from the chemical shift displacements upon the addition of paramagnetic lanthanide ions (Tb^{3+} or Tm^{3+}) or Y^{3+} as a diamagnetic reference.[10a] We practically tested the lanthanide ions from Tb^{3+} to Tm^{3+} first (8 to 12 electrons in f-orbitals), as they induce large PCS values for measurements. In case the accompanying line broadening arising from PRE effect becomes undesirable, other less paramagnetic lanthanides, for example, Yb^{3+} or Eu^{3+}, would be examined. The paramagnetic signals were assigned based on the collinear property[17] of the diamagnetic peak and the two paramagnetic peaks (Figure 2). The ambiguity of assigning paramagnetic peaks was further lifted by the ^{15}N edited NOESY-HSQC spectra (Figure S2) because the $^{1}H_N$-$^{1}H_N$ NOE### patterns were well predicted from the free-form crystal structure of the BRM bromodomain (PDB code: 4QY4). Facilitated by the combination of collinear properties and NOE patterns, a total of 35 and 36 protein-observed PCS values were measured for the C88A/K64C and C88A/L86C mutants, respectively.

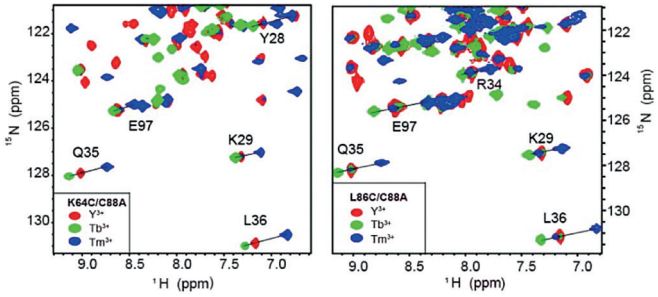

Figure 2. Pseudocontact shifts of the ^{15}N-labeled BRM bromodomain with a chemically modified lanthanide chelator. a) Superimposition of HSQC spectra of the C88A/K64C mutant in the presence of Y^{3+}, Tm^{3+}, or Tb^{3+}, respectively. b) Spectral overlay of the C88A/L86C mutant.

To measure the low-populated bound-state ligand ^{19}F PCSs, we acquired the ligand-observed ^{19}F CEST spectra of **1** (0.1 mM) in the presence of approximate 2.5 % (molar ratio) Tm^{3+}, Tb^{3+} and Y^{3+} labeled BRM bromodomain, respectively. The ^{19}F CEST used the ^{19}F presaturation pulse Scheme, with the saturation frequency scanned from approximately −4 to 10 ppm relative to the free-form ligand ^{19}F resonance. This range was optimized from an initial scanning over a large frequency range to determine the ^{19}F bound-state chemical shift. A weak ^{19}F B_1 field strength of 60 Hz with a duration of 0.8 s was applied during saturation to achieve a sufficient transfer from the low-populated bound-state to the free-state ^{19}F signals. These ^{19}F CEST spectra were acquired using an Agilent 500 MHz spectrometer equipped with a room-temperature ^{19}F probe. The ^{19}F CEST profiles, that is, the variations of the ^{19}F intensities of the free ligand with respect to the saturation frequencies, reveal two clear dips of the free and bound-state ^{19}F resonances (Figure 3 a,b). In a control experiment, the ^{19}F CEST profile showed no dip at other than the free-state ^{19}F frequency in the absence of protein (Fig-

 © 2017 Wiley-VCH Verlag GmbH & Co. KGaA, Weinheim

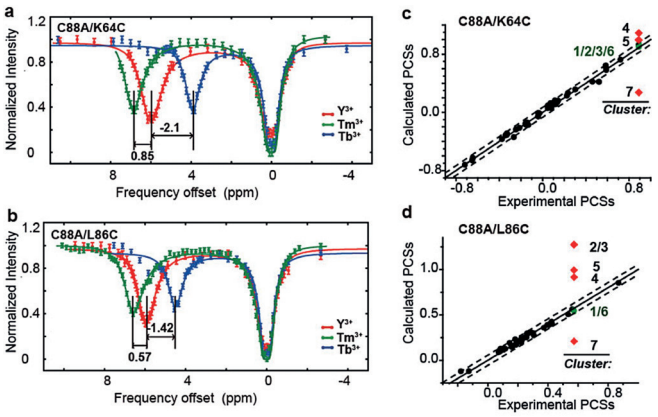

Figure 3. The low-populated bound-state ^{19}F PCSs and their correlation with those back-calculated from docking models of **1**. a) The CEST profiles of compound **1** in the presence of a low-populated C88A/K64C mutant of the BRM bromodomain, chelated with either paramagnetic lanthanide ion (Tb^{3+} or Tm^{3+}) or the diamagnetic Y^{3+} ion. The values of the bound-state ligand pseudocontact shifts are annotated in ppm. b) The CEST profile of **1** in the presence of the C88A/L86C mutant. c) Correlation between experimental and back-calculated PCSs of the ^{15}N-labeled C88A/K64C mutant of the BRM bromodomain and the ligand **1**. The protein-observed PCSs enables the determination of the magnetic susceptibility tensor, which in turn allows the back-calculation of the bound-state ^{19}F PCSs using the lowest-energy poses of the docking clusters. Dotted lines represent three standard deviations from the predicted protein-observed PCSs. d) PCS correlation in the case of the C88A/L86C mutant.

ure S3). The bound-state ^{19}F chemical shifts moved −2.1 or 0.85 ppm, upon titration of a small amount of the Tb^{3+} or Tm^{3+} labeled C88A/K64C mutant relative to the Y^{3+} labeled protein (Figure 3a). Accordingly, the bound-state ^{19}F chemical shift displacements of −1.42 and 0.57 ppm, that is, ^{19}F PCSs, were measured for the Tb^{3+} or Tm^{3+} labeled C88A/L86C mutant (Figure 3b). The ratios of the ^{19}F PCSs (about 2.5) induced by the Tb^{3+} or Tm^{3+} labeled proteins were consistent with those of the protein-observed ^{15}N PCSs. These bound-state ^{19}F PCSs are transferred from the lanthanide-labeled protein to the ligand, which carry valuable distance and angular information of vectors directing from the paramagnetic centers to the bound-state ^{19}F nuclei (Ln-F).

To back-calculate the bound-state ligand ^{19}F PCSs, we retrieved the Ln-F vectors from the ligand poses (DOCK6, UCSF) docking to the free-form BRM bromodomain (Figure S4). The lanthanide coordinates and associated magnetic susceptibility tensors (Table S1) of the two BRM mutants were accurately determined from the protein-observed ^{15}N PCSs, as indicated by the agreement between the experimental ^{15}N PCSs and the back-calculated PCSs from the free-form protein crystal structure using the Numbat[18] software (Figure 3c,d). The standard deviations were then estimated from the correlations of experimental and back-calculated ^{15}N PCSs. Using the two standard deviations as a threshold, the docking poses with predicted ^{19}F PCSs deviating more than the threshold were filtered out. The poses within a given cluster superimposed well with each other (Figure S4); thus, only the lowest-energy pose in each cluster was considered in the back-calculation of the ^{19}F PCSs. Clusters 1 and 6 are indistinguishable using this ^{19}F PCS-CEST approach (Figure S4), as the ^{19}F atoms in these two clusters were separated by only 0.2 Å. The rest of the unfavorable clusters were readily discriminated from the back-calculated bound-state ^{19}F PCSs of inhibitor **1** (Figure 3c,d).

To validate the protein–ligand interaction mode, we determined the ^{19}F bound-state PCSs of a di-fluorinated inhibitor (**2**) (Figure 4a). The ^{19}F CEST spectra were acquired using a Bruker 600 MHz spectrometer equipped with a cryoprobe to compensate for the relative lower aqueous solubility of inhibitor **2** (about 50 μM). The CEST profiles of the two fluorine atoms presented the chemical shifts of the free and bound state of compound **2** (Figure 4b,c), respectively. We then determined the bound-state ^{19}F PCSs in the presence of the low-populated BRM bromodomain, chelated with either the paramagnetic Tm^{3+} ion or the diamagnetic Y^{3+} ion. The docking pose 1 was then identified based on the agreement between the experimental and back-calculated PCSs of the two ^{19}F atoms of **2** simultaneously (Figure 4d, S5).

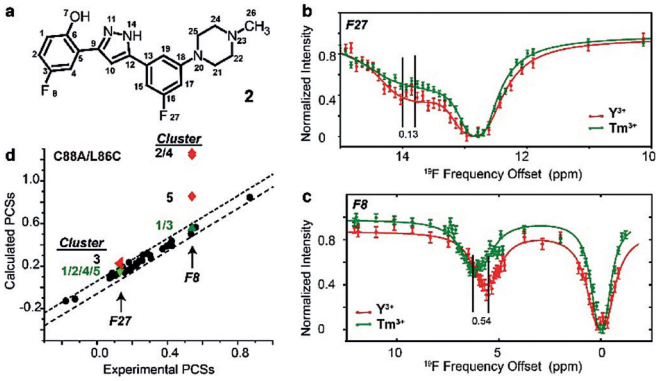

Figure 4. The low-populated bound-state ^{19}F PCSs of the di-fluorinated inhibitor **2**. a) Chemical structure of inhibitor **2**. b) The CEST profile of the F27 atom of inhibitor **2** in the presence of a low-populated lanthanide-labeled C88A/L86C mutant of the BRM bromodomain. c) The CEST profile of the F8 atom of inhibitor **2**. d) Correlation between experimental ^{19}F PCSs of inhibitor **2** and those back-calculated from docking poses.

To further corroborate the protein–ligand interaction modes delineated by ^{19}F PCS-CEST, we solved the crystal structure of the BRM bromodomain in complex with a more soluble analog (**3**), diffracted at a resolution of 1.8 Å (Figure 5a and Table S2). Compound **3** displaces four structured water molecules present in the free-form BRM bromodomain, and such a water-mediated interaction network is usually well conserved in other bromodomains.[19] The phenol oxygen of **3** forms a direct hydrogen bond with the side chain of residue Y1421, and the amide oxygen of **3** accepts another direct hydrogen bond from residue N1464 (Figure 5b). These two residues are well conserved among human bromodomains. Detailed structural chemical biology studies of the BRM bromodomain inhibitors will be elaborated elsewhere. The best-fitting poses of inhibitor **1** and **2** identified by the ^{19}F PCS-CEST approach superimposed well with each other, with the fluorobenzyl groups protruding into the acetyl-lysine

 © 2017 Wiley-VCH Verlag GmbH & Co. KGaA, Weinheim

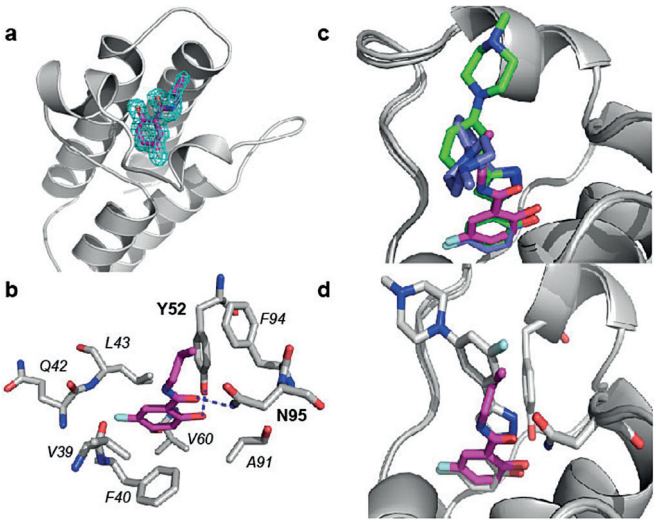

Figure 5. Structural insight into the BRM bromodomain in complex with inhibitors **1**–**3**. a) The crystal structure of the BRM bromodomain in complex with inhibitor **3**. The $2F_o-F_c$ electron density map is shown in blue mesh contoured at 1σ. b) The interaction details between the BRM bromodomain (carbon atoms colored in grey) and **3** (magenta). c) Superimposition of the BRM bromodomain-**3** (magenta) complex structure onto the docking results of inhibitor **1** (green or blue) filtered by the ^{19}F PCS-CEST approach. d) Superimposition of the BRM bromodomain-**3** (magenta) complex structure onto the docking results of inhibitor **2** (gray) filtered by the ^{19}F PCS-CEST approach.

recognition pocket of the BRM bromodomain. The positioning of the fluorobenzyl group of **1** and **2** was confirmed by the 0.5 and 0.6 Å deviations from the ^{19}F atom of **3**, respectively (Figure 5c,d).

The docking poses can alternatively be generated using XPLOR-NIH program containing the PARArestraints module driven by PCS restraints,[4] or using the PCS-driven HADDOCK.[20] The docking poses were hence generated using protein-observed ^{15}N PCSs, the bound-state ^{19}F PCSs, and the chemical shift perturbation data as experimental restraints in HADDOCK (Figure S6a, S6b). Since the number of bound-state ^{19}F PCSs is limited, a variety of poses were defined by docking energy terms. The PCSs back-calculated from the best-fitting pose agree well with the experimental ones (Figure S6c, S6d). Therefore, the bound-state ^{19}F PCSs is a useful filter of ligand poses generated using either DOCK or HADDOCK.

In conclusion, we have developed a new approach to interrogate protein–ligand interaction modes, despite the limit of NMR intermediate exchange. The outlined principles can be further extended to even larger proteins, in which the free-state ligand ^{19}F signals shall still be observable as the line broadening arising from the larger bound-sate ^{19}F chemical shift anisotropy and the intermediate chemical exchange can be both alleviated by the low protein–ligand ratio. The protein-observed methyl PCSs will allow the determination of lanthanide coordinates and associated magnetic susceptibility tensors, which in turn will enable the back-calculation of the low-populated bound-state ^{19}F PCSs. Once the magnetic susceptibility tensors are determined for a particular mutant, the ^{19}F bound-state PCSs can be readily retrieved for a variety of lead-like inhibitors using our ^{19}F PCS-CEST approach. It can also be potentially applied to the ^{13}C signals upon the availability of a highly soluble ligand or a ^{13}C labeled one, in which the possible homonuclear ^{13}C-^{13}C couplings should be taken into account for fitting the ^{13}C CEST profile. Our work paves the way for the structure-guided lead optimization of systems that were previously considered NMR inextricable.

Acknowledgements

We thank the staff at the BL17B/BL18U1/BL19U1 beamline of the National Center for Protein Sciences Shanghai (NCPSS) at the Shanghai Synchrotron Radiation Facility for their assistance during data collection. Part of our NMR work was performed at the National Center for Protein Sciences Shanghai, High Magnetic Field Laboratory and Key Laboratory of Magnet Resonance in Biological Systems, CAS. J.W. is financially supported by a grant from the Strategic Priority Research Program of the Chinese Academy of Sciences (XDB08030302). K.R. is financially supported by grants from the Ministry of Science and Technology of China (2016YFA0500700 and 2014CB910600) and the Natural Science Foundation of China (U1632153).

Conflict of interest

The authors declare no conflict of interest.

Keywords: chemical exchange saturation transfer · bromodomains · inhibitors · NMR spectroscopy · pseudocontact shifts

How to cite: *Angew. Chem. Int. Ed.* **2017**, *56*, 12982–12986
Angew. Chem. **2017**, *129*, 13162–13166

[1] H. Zheng, K. B. Handing, M. D. Zimmerman, I. G. Shabalin, S. C. Almo, W. Minor, *Expert Opin. Drug Discovery* **2015**, *10*, 975–989.
[2] M. P. Williamson, *Prog. Nucl. Magn. Reson. Spectrosc.* **2013**, *73*, 1–16.
[3] a) C. Eichmüller, W. Schuler, R. Konrat, B. Krautler, *J. Biomol. NMR* **2001**, *21*, 107–116; b) T. Brand, E. J. Cabrita, S. Berger, *Prog. Nucl. Magn. Reson. Spectrosc.* **2005**, *46*, 159–196.
[4] J.-Y. Guan, P. H. J. Keizers, W.-M. Liu, F. Loehr, S. P. Skinner, E. A. Heeneman, H. Schwalbe, M. Ubbink, G. Siegal, *J. Am. Chem. Soc.* **2013**, *135*, 5859–5868.
[5] a) M. Gochin, G. Zhou, A. H. Phillips, *ACS Chem. Biol.* **2011**, *6*, 267–274; b) J. Liu, J. Gao, F. Li, R. Ma, Q. Wei, A. Wang, J. Wu, K. Ruan, *Biochim. Biophys. Acta Gen. Subj.* **2017**, *1861*, 3061–3070; c) I. Bertini, M. Fragai, Y. M. Lee, C. Luchinat, B. Terni, *Angew. Chem. Int. Ed.* **2004**, *43*, 2254–2256; *Angew. Chem.* **2004**, *116*, 2304–2306.
[6] M. Reibarkh, T. J. Malia, G. Wagner, *J. Am. Chem. Soc.* **2006**, *128*, 2160–2161.
[7] a) D. E. Woessner, *J. Chem. Phys.* **1961**, *35*, 41–48; b) J. S. Leigh, *J. Magn. Reson.* **1971**, *4*, 308–311.
[8] P. Vallurupalli, G. Bouvignies, L. E. Kay, *J. Am. Chem. Soc.* **2012**, *134*, 8148–8161.
[9] a) G. Bouvignies, L. E. Kay, *J. Phys. Chem. B* **2012**, *116*, 14311–14317; b) T. Yuwen, A. Sekhar, L. E. Kay, *Angew. Chem. Int. Ed.*

 © 2017 Wiley-VCH Verlag GmbH & Co. KGaA, Weinheim

2016, *55*, 11490 – 11494; *Angew. Chem.* **2016**, *128*, 11662 – 11666; c) A. Sekhar, R. Rosenzweig, G. Bouvignies, L. E. Kay, *Proc. Natl. Acad. Sci. USA* **2016**, *113*, E2794 – E2801.

[10] a) G. Pintacuda, M. John, X.-C. Su, G. Otting, *Acc. Chem. Res.* **2007**, *40*, 206 – 212; b) M. A. S. Hass, M. Ubbink, *Curr. Opin. Struct. Biol.* **2014**, *24*, 45 – 53; c) S. P. Skinner, W.-M. Liu, Y. Hiruma, M. Timmer, A. Blok, M. A. S. Hass, M. Ubbink, *Proc. Natl. Acad. Sci. USA* **2015**, *112*, 9022 – 9027; d) L. de la Cruz, N. Thi Hoang Duong, K. Ozawa, J. Shin, B. Graham, T. Huber, G. Otting, *J. Am. Chem. Soc.* **2011**, *133*, 19205 – 19215; e) I. Bertini, C. Del Bianco, I. Gelis, N. Katsaros, C. Luchinat, G. Parigi, M. Peana, A. Provenzani, M. A. Zoroddu, *Proc. Natl. Acad. Sci. USA* **2004**, *101*, 6841 – 6846; f) I. Bertini, Y. K. Gupta, C. Luchinat, G. Parigi, M. Peana, L. Sgheri, J. Yuan, *J. Am. Chem. Soc.* **2007**, *129*, 12786 – 12794; g) I. Bertini, C. Luchinat, G. Parigi, E. Ravera, *NMR of Paramagnetic Molecules*, *Vol. 2*, 2nd ed., Elsevier Science, Amsterdam, **2016**, chap. 9.

[11] G. B. Crull, J. W. Kennington, A. R. Garber, P. D. Ellis, J. H. Dawson, *J. Biol. Chem.* **1989**, *264*, 2649 – 2655.

[12] P. Harvey, I. Kuprov, D. Parker, *Eur. J. Inorg. Chem.* **2012**, 2015 – 2022.

[13] R. S. Ma, Q. F. Li, A. D. Wang, J. H. Zhang, Z. J. Liu, J. H. Wu, X. C. Su, K. Ruan, *Phys. Chem. Chem. Phys.* **2016**, *18*, 13794 – 13798.

[14] P. Han, W. Li, C.-H. Lin, J. Yang, C. Shang, S. T. Nurnberg, K. K. Jin, W. Xu, C.-Y. Lin, C.-J. Lin, Y. Xiong, H.-C. Chien, B. Zhou, E. Ashley, D. Bernstein, P.-S. Chen, H.-S. V. Chen, T. Quertermous, C.-P. Chang, *Nature* **2014**, *514*, 102 – 106.

[15] a) B. G. Wilson, C. W. M. Roberts, *Nat. Rev. Cancer* **2011**, *11*, 481 – 492; b) E. C. Dykhuizen, D. C. Hargreaves, E. L. Miller, K. Cui, A. Korshunov, M. Kool, S. Pfister, Y.-J. Cho, K. Zhao, G. R. Crabtree, *Nature* **2013**, *497*, 624 – 627; c) T. Oike, H. Ogiwara, Y. Tominaga, K. Ito, O. Ando, K. Tsuta, T. Mizukami, Y. Shimada, H. Isomura, M. Komachi, K. Furuta, S.-I. Watanabe, T. Nakano, J. Yokota, T. Kohno, *Cancer Res.* **2013**, *73*, 5508 – 5518.

[16] M. Allegrozzi, I. Bertini, M. B. L. Janik, Y. M. Lee, G. H. Lin, C. Luchinat, *J. Am. Chem. Soc.* **2000**, *122*, 4154 – 4161.

[17] S. P. Skinner, M. Moshev, M. A. S. Hass, M. Ubbink, *J. Biomol. NMR* **2013**, *55*, 379 – 389.

[18] C. Schmitz, M. J. Stanton-Cook, X.-C. Su, G. Otting, T. Huber, *J. Biomol. NMR* **2008**, *41*, 179 – 189.

[19] T. D. Crawford, V. Tsui, E. M. Flynn, S. Wang, A. M. Taylor, A. Cote, J. E. Audia, M. H. Beresini, D. J. Burdick, R. Cummings, L. A. Dakin, M. Duplessis, A. C. Good, M. C. Hewitt, H.-R. Huang, H. Jayaram, J. R. Kiefer, Y. Jiang, J. Murray, C. G. Nasveschuk, E. Pardo, F. Poy, F. A. Romero, Y. Tang, J. Wang, Z. Xu, L. E. Zawadzke, X. Zhu, B. K. Albrecht, S. R. Magnuson, S. Bellon, A. G. Cochran, *J. Med. Chem.* **2016**, *59*, 5391 – 5402.

[20] C. Schmitz, A. M. J. J. Bonvin, *J. Biomol. NMR* **2011**, *50*, 263 – 266.

Manuscript received: July 12, 2017
Revised manuscript received: August 15, 2017
Accepted manuscript online: August 28, 2017
Version of record online: September 19, 2017

 © 2017 Wiley-VCH Verlag GmbH & Co. KGaA, Weinheim